Structural, elastic, and electronic properties of SiC, BN, and BeO nanotubes

Björn Baumeier,[*] Peter Krüger, and Johannes Pollmann

Institut für Festkörpertheorie, Universität Münster, D-48149 Münster, Germany

(Received 11 April 2007; revised manuscript received 26 June 2007; published 7 August 2007)

We present the results of a comparative *ab initio* study of single-walled SiC, BN, and BeO nanotubes (NTs) in zigzag and armchair configurations. Within density functional theory, we employ self-interaction-corrected pseudopotentials that were shown previously to yield reliable results for both structural and electronic properties of related bulk crystals. Using these pseudopotentials, we investigate the dependence of the atomic relaxation, strain energy, Young's modulus, and electronic structure on nanotube diameter and compound ionicity. Qualitatively, the NTs of all three wide-band-gap compounds show similar radially buckled geometries upon atomic relaxation, similar strain energy progressions with NT diameter and a saturation of Young's modulus as well as the band gap energy for large NT diameters. The band gap progression with NT diameter, which is of crucial importance for device applications, is presented and analyzed in detail. For SiC and BN, the calculated band gap energies of zigzag NTs vary much stronger for small and medium diameters than those of their armchair counterparts showing a significant narrowing of the band gaps. In contrast, the band gap progression in zigzag and armchair BeO NTs shows a very peculiar behavior for small diameters. No band gap breakdown occurs and the gap goes through a minimum for zigzag BeO NTs. The qualitative difference in the nature of the lower conduction band states in SiC and BN NTs, as compared to BeO NTs, and the increasing ionicity of these compounds are shown to be responsible for the observed effects.

PACS number(s): 73.22.−f, 73.63.Fg, 73.61.Ng, 61.46.Fg

I. INTRODUCTION

The initial discovery of carbon nanotubes (CNTs) by Iijima[1] in 1991 has sparked considerable interest in this kind of nanosized one-dimensional structures due to their unique physical properties and the associated potential for applications, e.g., in electronics and sensing. While experimental observations indicate that CNTs preferentially exist in multiwalled configurations with an interwall distance comparable to the spacing of planes in graphite, the generation of single-walled structures consisting of a single rolled-up graphene strip is technically feasible, as well. The chirality and diameter of such NTs are uniquely specified[2] by the pair of helical indices (n,m) defining the vector $\mathbf{c}_h = n\mathbf{a}_1 + m\mathbf{a}_2$, where $\mathbf{a}_1$, $\mathbf{a}_2$ are the unit vectors of a graphitic sheet.

In addition to CNTs, a considerable number of different composite nanoscale tubular structures has either already been fabricated, based on crystals such as BN, SiC, MoS_2, WS_2,[3–6] or suggested, as in the case of BeB_2 and B_2O,[7] BeO,[8] or MgO[9,10] NTs. Carbon, SiC, BN, and BeO NTs differ in their increasing ionicity. As a consequence, the properties of SiC, BN and BeO NTs are different from those of the covalently bonded, homopolar CNTs. Most notably, the electronic characteristics are strongly dependent on the type of chemical bonding in these solids. While CNTs have been found to be either metallic or semiconducting depending on their helicity,[2,11,12] previous studies have shown that both BN and SiC NTs are semiconducting, their structural as well as electronic properties depending in characteristic ways on the chirality and the diameter of the NTs.[13–27]

Theoretically, BN NTs have been studied quite intensively during the last decade on different levels of sophistication,[13] e.g., by tight-binding calculations,[13–15] density functional theory (DFT) within local density approximation,[13,16–19] (LDA) and hybrid functional calculations.[24] Studying exci-

tons in NTs, Park *et al.*[28] as well as Wirtz *et al.*[29] have more recently carried out *GW* quasiparticle energy calculations on a (8,0) or several selected BN NTs, respectively. SiC NTs and defects in SiC NTs have been addressed only in the last couple of years. DFT cluster or supercell calculations have been reported[20–23,25,26] and very recently H and its interaction with B acceptors and N donors in (8,0) zigzag and (5,5) armchair SiC NTs have been studied employing hybrid density functional calculations, as well.[27] Concerning BeO NTs, we are aware of only one very recent DFT-LDA study.[8]

An accurate determination of the band gap energy of NTs is crucial both for applications in electronic devices as well as from a more fundamental point of view. Within standard DFT-LDA, band gaps of semiconductors and insulators are significantly underestimated. Many of the studies reported so far for the NTs considered in this work suffer from the usual LDA shortcoming. To overcome this problem, we employ self-interaction-corrected (SIC) pseudopotentials whose construction has been described in detail before.[30–33] Employing these SIC pseudopotentials, we have previously obtained bulk and surface electronic properties for a variety of semiconductors and insulators in very good agreement with experimental data and with the results of considerably more elaborate quasiparticle calculations. Hence, we expect the SIC approach to yield a reliable description of electronic properties of NTs, as well.

In this paper we report a comprehensive account of *ab initio* DFT-SIC results on structural, elastic, and electronic properties of a large variety of SiC, BN, and BeO NTs in $(n,0)$ zigzag and (n,n) armchair configurations with n values ranging from 4 to 15 and diameters up to 25 Å, respectively. The numerical simplicity of our DFT-SIC approach allows us to easily study a large variety of NTs on equal footing. The calculated structural and elastic properties of SiC and BN NTs corroborate earlier tight-binding and the selected DFT-

LDA results. Only very few results on respective properties of BeO nanotubes have been reported to date.[8] Applying our DFT-SIC approach to the calculation of electronic NT properties of SiC, BN, and BeO NTs, we obtain significant improvements in the gap energies over standard DFT-LDA results for all nanotubes studied. Only the hybrid density functional calculations[24,27] and the *GW* quasiparticle calculations,[28,29] which are considerably more demanding than our DFT-SIC calculations, have arrived at similar gap energy values for a few selected SiC and BN NTs. In particular, we address a most quantitative analysis of the effects which the increasing ionicity of the chemical bond in these tubular nanostructures has on their physical properties and give a real-space analysis of the band gap progression with tube diameter.

The paper is organized as follows. In Sec. II, we briefly summarize the methodology of our calculations. In Sec. III A, we report structural and electronic properties of the underlying single graphitic sheets. Structural, elastic, and electronic properties of SiC, BN, and BeO NTs in zigzag and armchair configurations are addressed in Sec. III B. The optimal structural relaxation of these NTs is evaluated by total energy minimization and the dependence of their elastic and electronic properties on NT diameter is presented and discussed. A brief summary concludes the paper.

II. CALCULATIONAL DETAILS

We employ our nonlocal, norm-conserving *ab initio* SIC pseudopotentials[30–33] in separable Kleinman-Bylander form.[34] The standard pseudopotentials entering their construction are set up according to the prescription of Hamann.[37] We use the exchange-correlation functional of Ceperley and Alder,[35] as parametrized by Perdew and Zunger.[36] To expand the wave functions, we employ three shells of atom-centered Gaussian orbitals of s, p, d, and s^* symmetry per atom with appropriately determined decay constants.[38] The inclusion of both fairly localized and extended orbitals is necessary to achieve an appropriate representation of the localized ionic bond states on the NT cylinder as well as the exponential decay of the wave functions into vacuum. To appropriately describe also the nearly free electron state in the lower conduction bands characteristic for the hexagonal sheets, as previously discussed[39] for the case of BN, we place one shell of additional localized Gaussian orbitals of s, p, d, and s^* symmetry type with a decay constant of 0.18 atomic units on planes in vacuum 1.5 a above and below the hexagonal sheets, where a is the hexagonal lattice constant. Rolling up the sheets into nanotubes, one point of concern becomes immediately obvious. The additional orbital localization points inside and outside the tubes constitute separate tubes. That on the outside causes no problem. Inside the tubes, however, localization points originating from opposite sides of the NT can come very close to one another so that numerical instabilities could arise for small tube diameters. To avoid such instabilities, we place the additional Gaussian orbitals inside the tubes only along the tube axis.

The properties of SiC, BN, and BeO graphitic sheets and NTs are calculated within a supercell approach, using the

TABLE I. Anion-cation bond lengths (in Å) in SiC, BN and BeO graphitic sheets and bulk crystals, as resulting from LDA and SIC calculations. Experimental bulk-bond lengths are given for comparison.

| | graphitic layer | | bulk crystal | | |
	LDA	SIC	LDA	SIC	Exp.
SiC	1.76	1.77	1.87	1.89	1.89[a]
BN	1.41	1.43	1.54	1.56	1.56[b]
BeO	1.52	1.53	1.63	1.65	1.65[c]

[a]From Ref. 43.
[b]From Ref. 44.
[c]From Ref. 45.

efficient algorithm presented in Ref. 40. We use vacuum layers of approximately 12 Å thickness in the lateral directions of the respective systems so that unphysical interactions between neighboring sheets or NTs are avoided. In the case of the graphitic sheets, we perform Brillouin-zone integrations using 14 special **k** points in the irreducible wedge of the hexagonal zone generated according to the prescription of Monkhorst and Pack.[41] Six and ten uniformly distributed special **k** points along the NT axis are used for the treatment of zigzag and armchair NTs, respectively.

Lattice constants of the graphitic sheets are optimized by total energy minimization. For the NTs, the total energy is evaluated for different unit cell lengths, while the positions of the constituent atoms are allowed to relax until all components of the calculated Hellmann-Feynman and Pulay forces are smaller than 0.6 mRy/a_B. Based on the resulting total energy curves, ground-state properties are calculated and the electronic structure is determined based on the fully optimized geometry.[42]

III. RESULTS

In this section, we first summarize structural and electronic properties of the underlying graphitic SiC, BN, and BeO sheets, which serve as an important reference for respective NTs, before we address NT properties themselves in detail.

A. Graphitic sheets

The bond lengths for the three graphitic sheets, as resulting from our standard LDA and SIC calculations, are summarized in Table I. Respective bulk-bond lengths of wurtzite SiC and BeO as well as zinc-blende BN, as calculated previously,[31–33] are given for reference in Table I in comparison with experimental values. The bulk-bond lengths calculated within SIC are in very good accord with experiment, indeed. Therefore, we expect the bond lengths for the graphitic layers calculated within SIC to be very accurate, as well.

The energy gaps of SiC, BN, and BeO graphitic sheets are summarized in Table II. Respective calculated bulk band gaps are given in comparison with measured bulk band gaps

TABLE II. Fundamental band gap energies (in eV) of SiC, BN, and BeO graphitic sheets and wurtzite SiC and BeO as well as zinc-blende BN bulk crystals, resulting from LDA and SIC calculations. Experimental bulk gaps are given for comparison.

| | graphitic layer | | bulk crystal | | |
	LDA	SIC	LDA	SIC	Exp.
SiC	2.58	3.94	2.12	3.33	3.33[a]
BN	4.51	6.31	4.45	6.13	6.10[b]
BeO	5.73	8.72	7.41	10.50	10.6[c]

[a]From Ref. 43.
[b]From Ref. 46.
[c]From Ref. 47.

for reference, as well. The LDA bulk gaps underestimate the experimental gaps very significantly, as usual. On the contrary, the SIC bulk gaps are in very good agreement with experiment. In addition, the SIC bulk gap for the BN sheet of 6.3 eV is in good accord with the quasiparticle band gap of 6.0 eV, as calculated in Ref. 39, and in very good agreement with the band gap of 6.3 eV, as following from hybrid density functional calculations.[24] Hence, we expect our SIC band gaps for the three graphitic sheets to be very accurate, as well. Also the "ionic" X_{3c}-X_{1c} bulk band gap of SiC, for example, results from our calculations as 2.86 eV in reasonable agreement with experiment (3.08 eV) and with the results of two quasiparticle calculations yielding 3.18 or 3.25 eV, respectively (see Ref. 32). In general, we observe that the band gap increases for SiC and BN when going from the bulk crystals to the graphitic sheets while it decreases for BeO. This is intimately related to the basically different character of the chemical bond in heteropolar covalent as compared to ionic compounds. For BN, which is fairly ionic already, the crossover between these opposite tendencies is almost reached.

The electronic band structures of graphene and SiC, BN, as well as BeO graphitic sheets are shown in Fig. 1. In contrast to metallic graphene, which exhibits the well known characteristic degeneracy of π and π^* states at the Fermi level occurring at the K point of the hexagonal Brillouin zone, all three types of graphitic sheets investigated in this work are wide-band-gap semiconductors or insulators. The band gaps of the SiC and BN sheets are direct at K. The band gap of BeO is indirect with the valence band maximum (VBM) at K and the conduction band minimum (CBM) at Γ. Since the two atoms in the unit cell are not identical for SiC, BN, and BeO graphitic sheets, the aforementioned degeneracy of the π and π^* states is removed. As a consequence, the electronic properties of respective NTs can be expected to be qualitatively different from those of carbon NTs. We note in passing that the graphene band structure in the left panel of Fig. 1 resulting from our DFT-SIC calculations is in good agreement with the GW quasiparticle band structure reported by Miyake and Saito.[48]

For all three compounds, the valence bands consist of a low-lying anionic s band and three upper mostly anionic s, p bands. The latter originate in all three compounds from mixtures of anionic p and cationic s states. The uppermost of these s, p bands has mainly s, p_z character. Since the p_z orbitals are perpendicular to the graphitic layers their interaction is a fairly small π-π interaction giving rise to the weaker dispersion of these bands, as compared to the other two upper valence bands. The spatial dependence of the interaction of the p_z orbitals is the same as that of valence s orbitals. As a consequence, the low-lying s and the upper s, p_z valence bands of the compounds have very similar dispersions, as is most obvious in Fig. 1. The anion p_x, p_y orbitals, on the contrary, lie in the graphitic sheets giving rise to a significantly different and larger dispersion, therefore. The lowest conduction band in the SiC and BN sheets occurs at the K point of the hexagonal Brillouin zone and has cationic p_z character. The lowest conduction band of the highly ionic
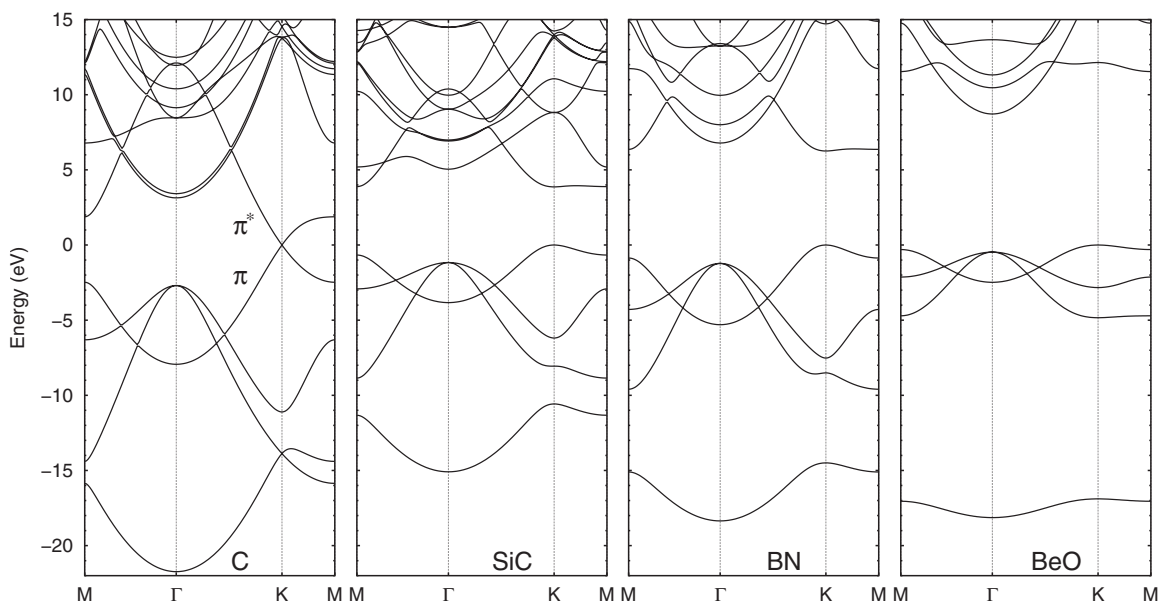
FIG. 1. Band structure of graphene and graphitic SiC, BN, and BeO sheets along the high-symmetry lines of the two-dimensional hexagonal Brillouin zone, referred to the Fermi level or to the top of the valence bands, respectively, as calculated within the SIC approach.
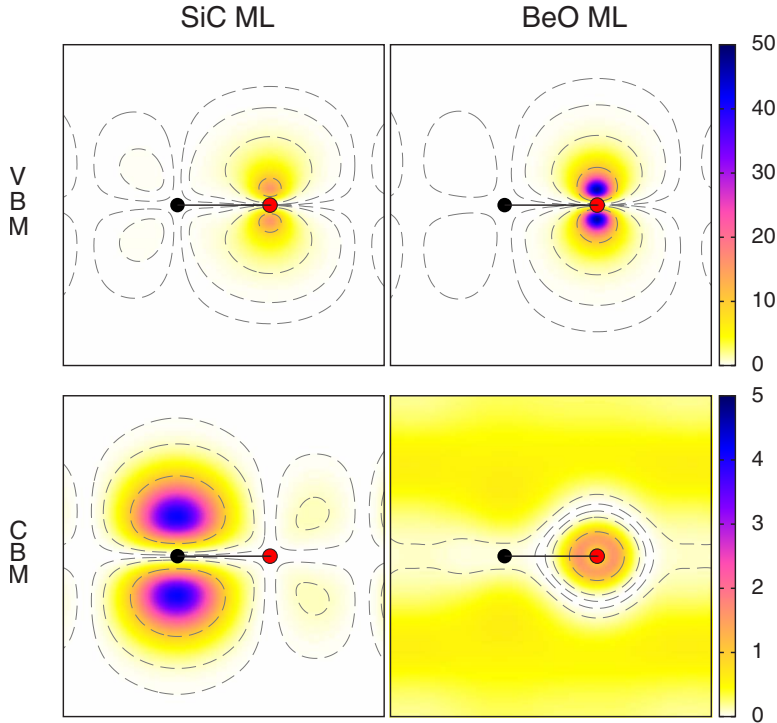
FIG. 2. (Color online) Charge density contours of the VBM and CBM states of graphitic SiC (left panels) and BeO (right panels) monolayers (in $10^{-2}a_B^{-3}$) plotted in the [110]-[001] plane containing the anion-cation bond, as calculated within the SIC approach. Anions and cations are depicted by red and black dots, respectively. The VBM and CBM states for SiC and the VBM state for BeO occur at the K point. The CBM state for BeO occurs at the Γ point.

BeO compound occurring at the Γ point, on the contrary, mainly originates from anion s orbitals. We note in passing that our band structure of the graphitic BN sheet in Fig. 1, in particular in the energy range from -10 to $+10$ eV, is in very good accord with the respective GW quasiparticle band structure as reported by Blase et al.[39]

The dispersion of the lowest conduction band of BeO is basically parabolic and thus nearly free-electron (NFE) like. The physical origin and the NFE character of the respective lowest conduction band at Γ in BN has been discussed in detail previously.[14,39]

The VBM states of the SiC and BN graphitic sheets are largely similar, as are the CBM states. The CBM state of the BeO graphitic sheet, on the contrary, shows very significant differences to the CBM states of the SiC and BN graphitic sheets. To highlight this difference, we compare in Fig. 2 the charge density contours of the VBM and CBM states of SiC and BeO graphitic sheets. The figure clearly reveals that the VBM state has anionic p_z character in both compounds giving rise to a fairly small dispersion of the respective uppermost valence band. The CBM state of the SiC graphitic sheet is of Si p_z character, as noted before, while that of the BeO sheet has O s character. It is largely different from the former state exhibiting its NFE character. This has important consequences for the electronic properties of BeO, as compared to SiC and BN NTs.

B. Nanotubes

In this section, we first briefly summarize structural and elastic properties of the investigated NTs in comparison with the pertinent literature and then turn to a more detailed discussion of their electronic properties.

1. Structural and elastic properties

When strips of graphitic SiC, BN, or BeO sheets are rolled up into single cylindrical tubes the anions and cations

relax from their ideal atomic positions. The cations move slightly inward towards the tube axis, while the anions move outward with respect to their ideal positions. This reduces the total energy of the system since the electron-electron repulsion is lowered. As a result, the NT surface becomes buckled. After relaxation, the radial geometry of the tubular structures is characterized by two concentric cylindrical tubes, with an outer anionic and an inner cationic cylinder. The strength of the buckling is defined by the radial buckling parameter

$$\beta = \bar{r}_a - \bar{r}_c, \qquad (1)$$

where $\bar{r}_a$ and $\bar{r}_c$ are the mean radii of the anion and cation cylinders, respectively. The values for the radial buckling resulting from our SIC calculations are shown in Fig. 3. For more quantitative comparisons they are summarized in Table III, as well. Obviously, there is no dependence of β on NT helicity in all three cases. For BN NTs this fact has been observed previously already by Hernández et al.[15] For all three compounds, the radial buckling decreases with increasing NT diameter and vanishes in the limit of very large NT diameters. The absolute values for β are larger for SiC than for BeO and BN NTs, which can basically be explained by the larger Si-C bond length (see Table I).

Next we address the strain energy necessary to form a NT, i.e., the energy per atom necessary to roll up the graphitic strip into tubular form. It is defined as the difference in total energy per atom between a NT and the respective graphitic sheet

$$E_s = \frac{1}{N_{\mathrm{NT}}}E_{\mathrm{NT}}^{\mathrm{tot}} - \frac{1}{2}E_{\mathrm{sheet}}^{\mathrm{tot}}, \qquad (2)$$

where N_{NT} is the number of atoms in the NT unit cell.
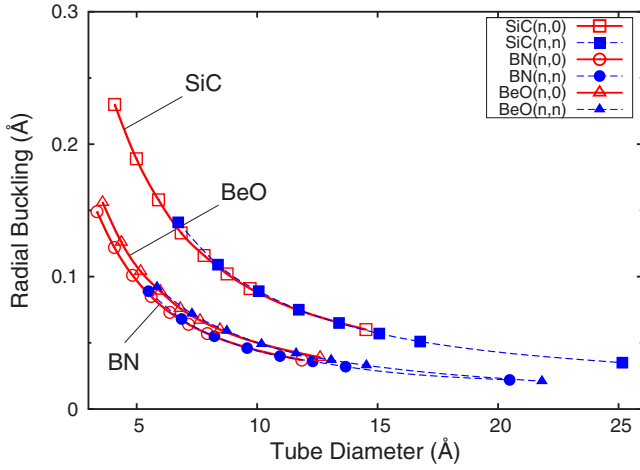
FIG. 3. (Color online) Radial buckling β (in Å) of $(n,0)$ zigzag (open symbols) and (n,n) armchair (filled symbols) SiC, BeO, and BN NTs as functions of the tube diameter d. Squares, triangles, and circles represent results for SiC, BeO, and BN, respectively. The solid and dashed lines are drawn to guide the eye.

In Fig. 4 the strain energy resulting from our SIC calculations is plotted as a function of the average tube diameter. Respective values are also summarized in Table III. The strain energies for SiC and BN NTs in Fig. 4 are fairly similar. For BeO NTs it is significantly lower (up to about d ~ 12 Å) due to the much higher ionicity of this compound, as compared to SiC and BN. Rolling respective sections of graphitic BeO layers up into NTs needs less energy, as can be inferred from the band structure and the charge densities of the graphitic BeO layer (see Figs. 1 and 2). The O $2p_z$ valence band is very narrow. The charge density of the CBM state is mainly localized at the O atoms. Around the Be atoms it is fairly smooth and small. In all three cases, the strain energy approaches zero for large NT diameters only very slowly since the NTs become equivalent to graphitic sheets only for very large diameters. Figure 4 shows that the strain energy is also independent of the NT helicity. Its progression resembles a classical $\sim d^{-2}$ law. For BN NTs, our *ab initio* results calculated within the SIC framework corroborate respective values calculated previously within tight-binding,[14] nonorthogonal tight-binding,[15] or standard LDA.[16,21,22] For SiC NTs, our calculated progression of the strain energy with tube diameter is in good agreement with that calculated by Zhao *et al.*[23] within DFT-LDA.

Another interesting structural feature of NTs is their behavior under uniaxial strain along the NT axis. It is described by Young's modulus, which is conventionally defined as the second derivative of the total energy with respect to the strain ϵ

$$Y = \frac{1}{V_0} \left. \frac{\partial^2 E}{\partial \epsilon^2} \right|_{\epsilon=0}, \qquad (3)$$

where V_0 is the equilibrium volume. As the volume for a hollow cylinder is $V_0 = 2\pi L R \delta R =: S_0 \delta R$ it is necessary to adopt a certain convention for the shell thickness δR in the case of single-walled NTs. Here we follow the suggestion of

TABLE III. Structural, elastic, and electronic properties of SiC, BN, and BeO NTs. Tube diameters d and radial buckling parameters β are given in Å, strain energies E_s in eV per atom, modified Young's moduli Y_s in TPa nm, and band gap energies E_g in eV.

(n,m)	d	β	E_s	Y_s	E_g
SiC					
(4,0)	4.09	0.230	0.396	0.115	0.62
(5,0)	4.99	0.189	0.238	0.143	1.16
(6,0)	5.90	0.158	0.169	0.149	1.81
(7,0)	6.85	0.133	0.129	0.154	2.38
(8,0)	7.80	0.116	0.104	0.156	2.56
(9,0)	8.75	0.102	0.087	0.160	2.81
(10,0)	9.71	0.091	0.075	0.161	3.04
(15,0)	14.52	0.060	0.046	0.166	3.42
(4,4)	6.73	0.141	0.121	0.157	3.14
(5,5)	8.38	0.109	0.087	0.162	3.47
(6,6)	10.07	0.089	0.067	0.164	3.49
(7,7)	11.73	0.075	0.056	0.165	3.63
(8,8)	13.40	0.065	0.048	0.166	3.65
(9,9)	15.07	0.057	0.043	0.167	3.72
(10,10)	16.77	0.051	0.039	0.168	3.74
(15,15)	25.16	0.035	0.030	0.168	3.78
BN					
(4,0)	3.35	0.149	0.479	0.227	3.04
(5,0)	4.08	0.122	0.301	0.246	3.45
(6,0)	4.83	0.101	0.218	0.259	3.95
(7,0)	5.60	0.085	0.171	0.263	4.78
(8,0)	6.37	0.073	0.140	0.267	4.89
(9,0)	7.15	0.064	0.118	0.269	5.25
(10,0)	7.99	0.057	0.102	0.273	5.51
(15,0)	11.85	0.037	0.063	0.278	5.83
(4,4)	5.49	0.089	0.168	0.268	5.75
(5,5)	6.87	0.068	0.123	0.272	5.72
(6,6)	8.23	0.055	0.096	0.274	6.06
(7,7)	9.59	0.046	0.080	0.275	6.08
(8,8)	10.95	0.040	0.069	0.276	6.11
(9,9)	12.31	0.036	0.061	0.277	6.22
(10,10)	13.67	0.032	0.055	0.278	6.24
(15,15)	20.48	0.022	0.041	0.279	6.27
BeO					
(4,0)	3.59	0.156	0.208	0.095	8.69
(5,0)	4.37	0.126	0.134	0.107	8.16
(6,0)	5.17	0.104	0.100	0.111	7.86
(7,0)	5.98	0.089	0.079	0.117	7.71
(8,0)	6.81	0.076	0.067	0.119	7.67
(9,0)	7.63	0.067	0.058	0.121	7.78
(10,0)	8.46	0.060	0.052	0.122	8.03
(13,0)	9.95	0.052	0.044	0.123	8.65
(15,0)	12.61	0.039	0.038	0.125	8.70
(4,4)	5.85	0.092	0.077	0.124	7.27
(5,5)	7.30	0.072	0.058	0.123	7.75

TABLE III. (*Continued.*)

(n,m)	d	β	E_s	Y_s	E_g
(6,6)	8.74	0.059	0.049	0.124	8.17
(7,7)	10.18	0.049	0.043	0.126	8.65
(8,8)	11.62	0.042	0.040	0.126	8.73
(9,9)	13.07	0.037	0.037	0.127	8.75
(10,10)	14.54	0.033	0.035	0.127	8.77
(15,15)	21.82	0.021	0.032	0.128	8.78

Ref. 15 and describe the NT stiffness independent of δR by a modified Young's modulus

$$Y_s = \frac{1}{S_0} \left. \frac{\partial^2 E}{\partial \epsilon^2} \right|_{\epsilon=0}, \tag{4}$$

which is related to the standard Young's modulus by $Y_s = Y \delta R$. In Fig. 5 we show the progression of the calculated values for Y_s with NT diameter. Respective values are summarized in Table III. For BN, SiC, and BeO NTs the modified Young's moduli reach saturation already at fairly small diameters $d \sim 10$ Å. Significant differences between armchair and zigzag configurations are not to be noted. The saturation values of Y_s are 0.28, 0.17, and 0.13 TPa nm for BN, SiC, and BeO, respectively. Those for BeO NTs are smallest which correlates with the low strain energies (see Fig. 4). The ratio of the Young's moduli for BN and SiC NTs is in good agreement with that of the bulk moduli of BN and SiC. Our results corroborate the respective tight-binding results of Hernández *et al.*[15] They are in quantitative agreement with the few DFT-LDA values given in the latter reference. The deviations between our *ab initio* results and the tight-binding results[15] are in the order of 2% for the NT diameters and about 10% for the Young's moduli. We note in passing that we have also calculated all structural and elastic properties of the NTs presented above within standard LDA. Since struc-
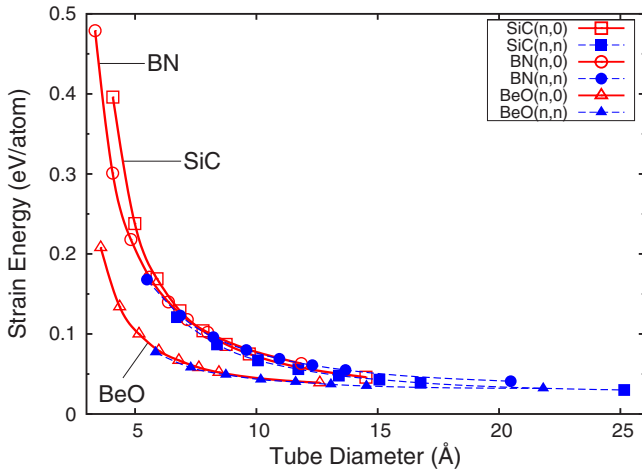
FIG. 4. (Color online) Strain energy of SiC, BN, and BeO $(n,0)$ zigzag (open symbols) and (n,n) armchair (filled symbols) NTs as functions of the tube diameter d. See caption of Fig. 3 for further details.
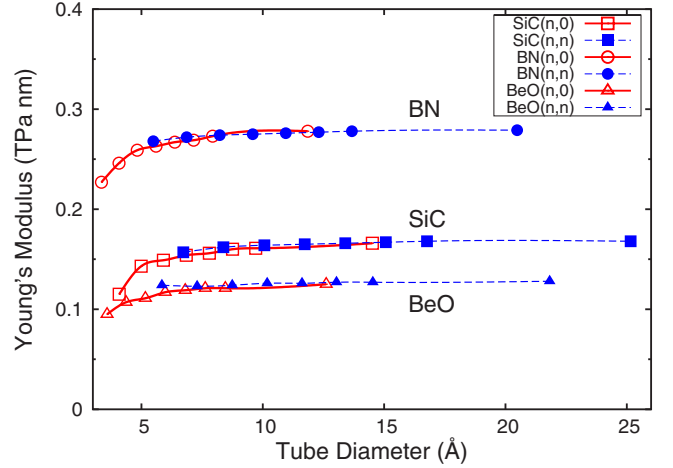
FIG. 5. (Color online) Modified Young's moduli Y_s (in TPa nm) of $(n,0)$ zigzag and (n,n) armchair BN, SiC, and BeO NTs as a function of the tube diameter d. See caption of Fig. 3 for further details.

tural properties follow from DFT-LDA with a good level of confidence (see Table I), only small deviations up to 1% occur.

2. Electronic properties

Most fundamentally, it turns out that all SiC, BN, and BeO NTs investigated are semiconducting, as was to be expected on the basis of the electronic properties of the respective graphitic sheets. They span a huge range of band gap energies from 0.5 to about 9 eV. Thus many nanoelectronic applications employing band gap energies of such a large range are conceivable. The band gaps are direct at Γ for $(n,0)$ zigzag NTs—with the notable exception of the (4,0) NTs—and indirect for (n,n) armchair NTs. The band structure of the NTs results from backfolding of the graphitic sheet bands onto the Γ-X line of the one-dimensional NT Brillouin zone and concomitant band splittings and shifts due to scattering of the sheet electrons at the NT lattice whose symmetry is reduced with respect to the sheets. This backfolding increases the number of bands drastically for large n. Figure 6 shows a few exemplary results. The SiC and BN (10,0) zigzag NTs exhibit a direct gap at Γ while the SiC and BeO (6,6) armchair NTs show indirect gaps from a k point on the Γ-X line to the X point or the Γ point of the one-dimensional Brillouin zone in the former or latter case, respectively. Our band structure for the BeO (6,6) armchair NT is in good agreement with the respective DFT-LDA result reported in Ref. 8 with the notable exception that our band gap is approximately 3 eV larger than the one reported in the latter reference.

Figure 7 shows the progression of the band gaps with tube diameter. The respective values are summarized for further comparison in Table III, as well. Several interesting features are to be noted. First, there is a qualitative similarity regarding the evolution of the band gaps in SiC and BN NTs. Both show significant differences between zigzag and armchair configurations, i.e., very pronounced helicity effects although their structural and elastic properties are virtually indepen-
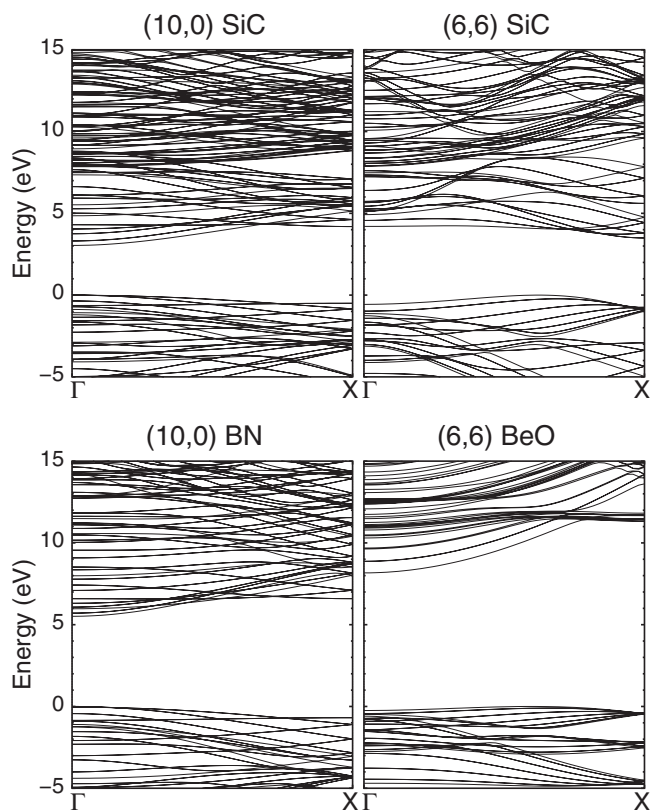
FIG. 6. Sections of the band structure of SiC and BN (10,0) zigzag as well as SiC and BeO (6,6) armchair NTs along the high-symmetry line Γ-X of the one-dimensional NT Brillouin zone. All energies are referred to the VBM which is defined as the zero of the energy scale.

dent of helicity. The same general behavior was found by Zhao *et al.*[23] for SiC NTs and by Okada *et al.*,[18] Xiang *et al.*,[21] and Guo *et al.*[22] for BN NTs in their DFT-LDA results. The absolute band gap values reported previously,[18,21–23] however, are significantly smaller than our values due to the well known underestimate of band gaps in LDA. It is interesting to note that the deviations between our band gap val-
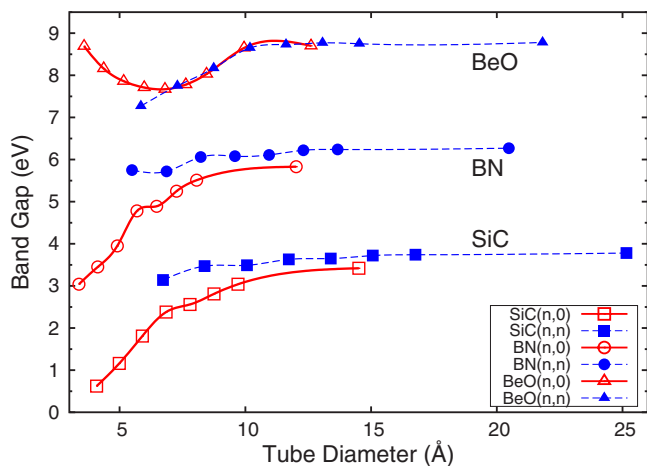
FIG. 7. (Color online) Fundamental gap of SiC, BN, and BeO $(n,0)$ zigzag and (n,n) armchair NTs as functions of the tube diameter d. See caption of Fig. 3 for further details.

ues and those of Okada *et al.*[18] and Guo *et al.*[22] are not constant but span a range from about 1 to 1.7 eV showing that it is not fully appropriate to just apply the same constant upward shift to the LDA conduction bands of all NTs as is often conjectured. The band gaps calculated within hybrid density functional theory for SiC NTs (Ref. 27) and BN NTs,[24] on the contrary, are in good accord with our results. For example, Gali[27] finds gap energies of 2.28 and 3.30 eV for (8,0) and (6,6) SiC NTs, respectively, to be compared to our values of 2.56 and 3.49 eV and Xiang *et al.*[24] report gap energies of about 6.2 eV for armchair BN NTs with diameters larger than 12 Å which compare favorably with our respective values for the (9,9), (10,10), and (15,15) BN NTs, respectively (see Table III). For large NT diameters our calculated band gaps converge towards the limiting values of the band gaps of the respective graphitic sheets. For smaller diameters, the band gaps of SiC and BN armchair tubes show only a small dependence on tube diameter while those of the zigzag tubes exhibit a strong diameter dependence. For very small diameters, the differences of their gap energy from that of the respective graphitic sheets is very pronounced, indeed. In particular, the gap of SiC zigzag tubes reduces dramatically with decreasing diameter almost approaching a band gap collapse. The different band gap progressions of zigzag and armchair NTs is related to different changes in the bonding and charge density topology in the NTs with respect to those in the graphitic sheets as we will discuss below.

In contrast, the progression of the band gap energy of BeO NTs is remarkably different (see Fig. 7). First of all, there is no discernible difference between zigzag and armchair tubes, except for the (7,0) zigzag and (4,4) armchair NTs. Second, for zigzag NTs of very small diameter, the gap is not strongly reduced, as in the case of SiC and BN, but goes through a minimum and opens up again, instead. In Ref. 8 the authors conclude on the basis of their DFT-LDA results that the band gap of BeO NTs is independent of chirality. Our results confirm this notion for zigzag and armchair NTs. At the same time, the authors conclude that the band gap is independent of the NT diameter amounting to about 5 eV for all BeO NTs considered.[8] Our results clearly reveal that this latter conclusion does not apply. Instead, the gap energies depend on nanotube diameter for $d \lesssim 10$ Å and their values range from 7.3 to 8.8 eV (see Fig. 7 and Table III).

Figure 8 shows the calculated VBM and CBM energies (full symbols) of all investigated zigzag SiCNTs, referred to the vacuum level $E_{\text{vac}}^{\text{sheet}}$ of the SiC graphitic sheet as the common energy reference. In addition, the open symbols represent the respective energy positions as resulting from simply backfolding the graphitic sheet bands. The figure clearly reveals that the dominant contribution to the gap narrowing originates from a change of the energy position of the lowest conduction band occurring as a consequence of the increasing NT curvature. In particular, the energy decrease of the CBM turns out to be entirely monotonous. The variation of the energy position of the VBM, on the contrary, is not monotonous for small diameters $d < 10$ Å. The differences between the monotonous CBM and the nonmonotonous VBM curves explains the discontinuous slope of the band gap progression for zigzag SiC NTs, as shown in Fig. 7. This peculiar progression is thus related to the more intricate de-
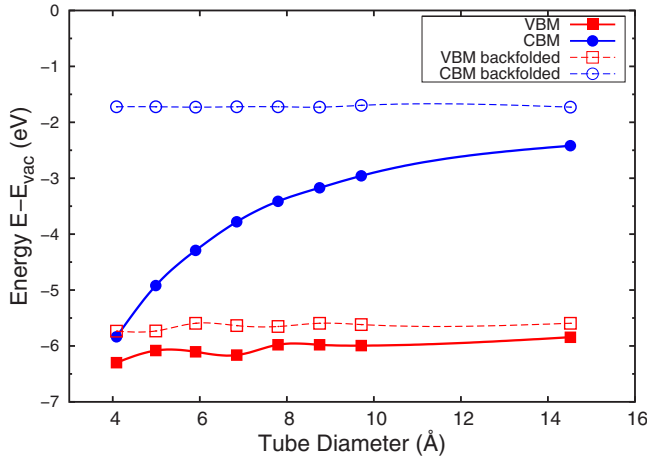
FIG. 8. (Color online) Progression of the VBM and CBM energies in zigzag SiC NTs as a function of tube diameter d. Full symbols result from NT calculations while the open symbols follow from backfolding the bands of the graphitic SiC sheet. The solid and dashed lines are drawn to guide the eye.

pendence of the VBM on NT diameter for small diameters and the respective discontinuous change of the neighbor configurations and interactions between occupied atomic orbitals across the interior of the NT cylinder.

To elucidate the physical origin of the particular band gap progressions in SiC, BN, and BeO NTs, we first address the qualitatively similar progressions for SiC and BN NTs (see Fig. 7) focussing on SiC NTs, for that matter. Thereafter, we discuss the band gap progression for BeO NTs.

While most of the previous literature on BN NTs discusses the origin of the band gap progression with tube diameter in **k** space,[13–19] we follow here a complementary line of reasoning by addressing its origin in real space using SiC and BeO NTs as examples. When a strip of graphitic SiC is rolled up into a NT, changes in the charge density occur. These are different for zigzag and armchair NTs because of their fundamentally different geometry. The charge densities of the VBM and CBM states of the graphitic SiC sheet, shown in the left panels of Fig. 2, reveal their anionic and cationic p_z character, respectively. When rolling the strip up into tubular form its curvature generally decreases the distance between neighboring sites to a certain extent. Much more importantly, the respective charge densities start to overlap inside the cylinder. Especially for zigzag NTs, this is a very pronounced effect while it is much smaller for armchair NTs. This is illustrated in Fig. 9 by charge density contours of the CBM state at the K point for the (5, 5) armchair and at the Γ point for the (9, 0) zigzag SiCNT. We concentrate in the following on the CBM states because they are mainly responsible for the band gap narrowing, as shown above. In both cases, the contours are drawn in a plane perpendicular to the NT axis containing an anion-cation ring for the armchair and a cation ring of the double-ring structure for the zigzag NT because the latter gives rise to the CBM. One can see that in the armchair NT (upper panel), the charge density remains localized at the cations and is distorted on the inner side of the ring only slightly in the bond direction towards the anions due to the curvature of the NT. In con-
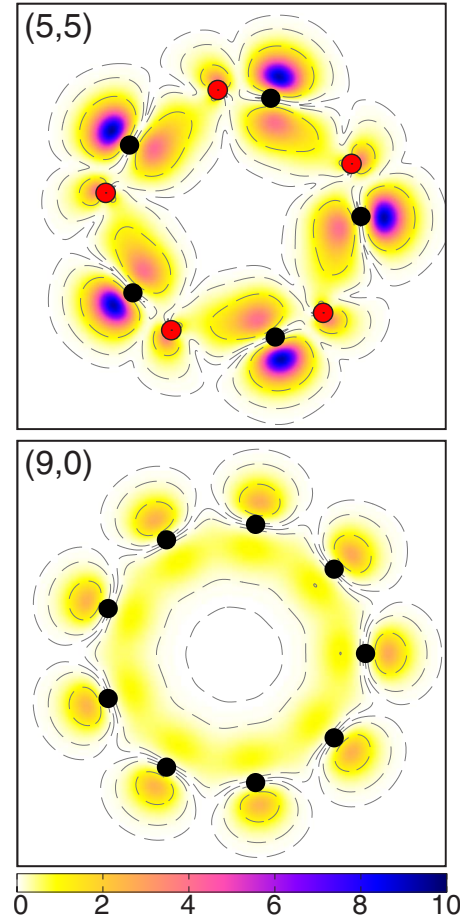
FIG. 9. (Color online) Charge density contours of the CBM states (in $10^{-3}a_B^{-3}$) of the one-dimensional Brillouin zone at the K point of a (5,5) armchair (upper panel) and the Γ point of a (9,0) zigzag (lower panel) SiC NT. The contours are drawn in planes perpendicular to the NT axis containing an anion-cation ring for the armchair and a cation ring for the zigzag NT. Anions and cations are again depicted by red and black dots, respectively.

trast, the charge density contour of the (9, 0) zigzag SiCNT (lower panel) very clearly demonstrates that a major redistribution of the charge density takes place inside the tube building up a ringlike distribution. The former p_z components of the charge density on the SiC graphitic sheet are pushed towards each other and a significant rehybridization leads to a ringlike charge density on the inner side of the tube. The former atomic character of the sheet states is entirely lost on the inner side of the NT. The CBM energy is lowered, therefore, and the fundamental energy gap is reduced with respect to the graphitic sheet. The p_z components of the cation orbitals on the outside of the NT are only slightly affected showing even less coupling between neighboring cations on the ring than in the graphitic sheet. The effects described above are even more pronounced for NTs with smaller diameters giving rise to an even stronger band gap reduction. Respective charge-density contours of the CBM state of (4, 0), (8, 0), and (10, 0) zigzag SiCNTs at the Γ point are compared in the left panels of Fig. 10. Note the dramatic increase of the charge density within the nanotube when n is decreased from 10 to 4.
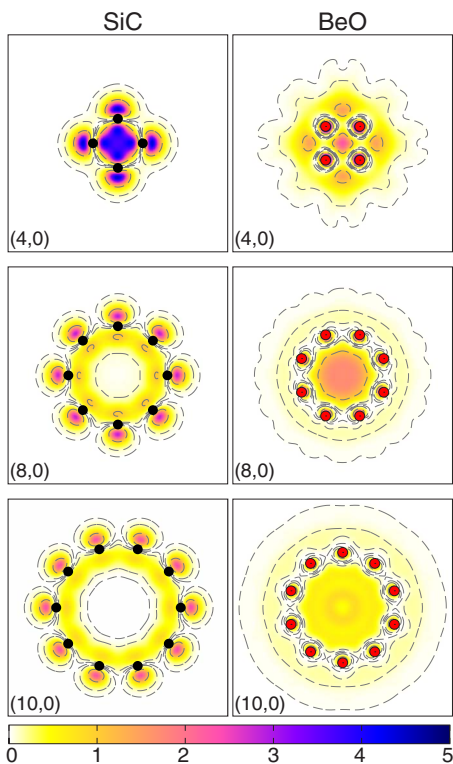
FIG. 10. (Color online) Charge density contours of the CBM states (in $10^{-3}a_B^{-3}$) at the Γ point of the one-dimensional Brillouin zone of (4,0), (8,0), and (10,0) SiC (left panels) and BeO (right panels) zigzag NTs. The charge densities for SiC and BeO NTs are plotted in a plane perpendicular to the NT axis containing a Si or an O ring, respectively, since the CBM of zigzag SiC NTs is made up of Si p orbitals, while that of zigzag BeO NTs is made up of O s orbitals. For further details, see caption of Fig. 9. Note that all charge densities are plotted on the same absolute scale so that they can be compared quantitatively.

In contrast, the insensitivity of the gap of BeO NTs to helicity seems to be related to the particular charge density topology of the CBM state in the graphitic BeO sheet (see the lower right panel of Fig. 2). The bottom of the conduction bands in BeO NTs originates from localized O s and very extended Be $2s$ states (of NFE character) which are not strongly influenced by rolling up the graphitic BeO strip into zigzag or armchair NTs. Thus, there is no helicity-induced difference in the gaps of both types of NTs. The peculiar dependence of the gap on NT diameter showing a minimum at a value of about 7 Å for the (8, 0) NT is more intricate. The charge density of the CBM state in $(n,0)$ zigzag BeO NTs is shown for $n=4$, 8, and 10 in the right panels of Fig. 10. The figure clearly reveals the different character of the CBM states of the BeO NTs (right panels), as compared to the respective CBM states of the corresponding SiC NTs (left panels). Generally speaking, an increasing interaction between second-nearest neighbors, i.e., between anions or cations across their respective rings, respectively, broadens corresponding anion- and cation-derived bands. As a result, the

energy gaps between the related bands become smaller. For armchair SiC NTs, e.g., there is no interaction across the interior of the NT cylinder (see the upper panel in Fig. 9) so that the gap energy remains close to its sheet value. For zigzag SiC NTs (see the left panels in Fig. 10) the interaction is minimal for the (10, 0) NT and increases down to the (4, 0) NT. Thus the gap decreases with decreasing n or tube diameter d, respectively, and is smallest for the (4, 0) zigzag SiC NT. For BeO zigzag NTs, on the contrary (see the right panels of Fig. 10), the interaction across the interior of the tube cylinder is small for the (10, 0) NT, becomes largest for the (8, 0) NT and becomes smaller again for the (4, 0) NT. Thus the (8, 0) zigzag BeO NT has the smallest gap.

IV. SUMMARY

We have reported a comprehensive comparison of structural, elastic, and electronic properties of compound semiconductor nanotubes with increasing ionicity, as studied by *ab initio* density functional theory employing self-interaction-corrected pseudopotentials which yield accurate band gaps, in particular. The progression of the radial buckling, strain energy, Young's modulus and energy gap with NT diameter has been investigated and related to the increasing ionicity of the SiC, BN, and BeO NTs considered. For all zigzag and armchair NTs investigated, we find that the structural and elastic properties are largely independent of NT helicity while the electronic structure of SiC and BN NTs very sensitively depends on it. This is not the case for BeO NTs. The origin of the peculiar helicity dependence of the gap energy in SiC and BN zigzag NTs and its helicity independence in BeO NTs has been analyzed in detail. In particular, we have elucidated why no large band gap narrowing occurs for small diameter zigzag BeO NTs, as opposed to zigzag SiC and BN NTs. To this end, we have analyzed the nature and origin of the band gap progressions and the peculiar differences of it between SiC and BN NTs, as compared to BeO NTs, by considering most relevant charge density contours which highlight crucial differences between the respective NTs and allow us to explain the different progressions of E_g in SiC and BN NTs, as compared to BeO NTs. The structural and elastic properties of SiC and BN NTs, as resulting from our *ab initio* calculations, are in good agreement with previous DFT-LDA results and corroborate respective earlier tight-binding results on BN NTs. For BeO NTs, our results appear to be the first comprehensive account of their structural and elastic properties. Concerning electronic properties of SiC, BN, and BeO NTs, our results confirm the qualitative outcome of previous tight-binding and DFT-LDA calculations and are in quantitative accord with selected hybrid density functional results on a few SiC and BN NTs available in the literature. This should be valued in view of the fact that our DFT-SIC calculations, treating all NTs studied on equal footing, are numerically not more demanding than any standard DFT-LDA calculation on NTs.

*baumeier@uni-muenster.de

[1] S. Iijima, Nature (London) **354**, 2148 (1991).

[2] R. Saito, M. Fujita, G. Dresselhaus, and M. S. Dresselhaus, Appl. Phys. Lett. **60**, 2204 (1992).

[3] N. G. Chopra, R. J. Luyken, K. Cherry, V. H. Crespi, M. L. Cohen, S. G. Louie, and A. Zettl, Science **269**, 966 (1995).

[4] X. H. Sun, C. P. Li, W. K. Wong, N. B. Wong, C. S. Lee, S. T. Lee, and B. K. Teo, J. Am. Chem. Soc. **124**, 14464 (2002).

[5] R. Tenne, L. Margulis, M. Genut, and G. Hodes, Nature (London) **360**, 444 (1992).

[6] R. Tenne, M. Homyonfer, and Y. Feldman, Chem. Mater. **10**, 3225 (1998).

[7] P. Zhang and V. H. Crespi, Phys. Rev. Lett. **89**, 056403 (2002).

[8] P. B. Sorokin, A. S. Fedorov, and L. A. Chernozatonskii, Phys. Solid State **48**, 398 (2006).

[9] A. N. Enyashin, I. R. Shein, and A. L. Ivanovskii, Phys. Rev. B **75**, 193408 (2007).

[10] I. R. Shein, A. N. Enyashin, and A. L. Ivanovskii, Phys. Rev. B **75**, 245404 (2007).

[11] N. Hamada, S. I. Sawada, and A. Oshiyama, Phys. Rev. Lett. **68**, 1579 (1992).

[12] X. Blase, L. X. Benedict, E. L. Shirley, and S. G. Louie, Phys. Rev. Lett. **72**, 1878 (1994).

[13] see, e.g., L. Vaccarini, C. Goze, L. Henrard, E. Hernández, P. Bernier, and A. Rubio, Carbon **38**, 1681 (2000), and references therein.

[14] A. Rubio, J. L. Corkill, and M. L. Cohen, Phys. Rev. B **49**, R5081 (1994).

[15] E. Hernández, C. Goze, P. Bernier, and A. Rubio, Phys. Rev. Lett. **80**, 4502 (1998).

[16] X. Blase, A. Rubio, S. G. Louie, and M. L. Cohen, Europhys. Lett. **28**, 335 (1994).

[17] Y.-H. Kim, K. J. Chang, and S. G. Louie, Phys. Rev. B **63**, 205408 (2001).

[18] S. Okada, S. Saito, and A. Oshiyama, Phys. Rev. B **65**, 165410 (2002).

[19] S.-H. Jhi, D. J. Roundy, S. G. Louie, and M. L. Cohen, Solid State Commun. **134**, 397 (2005).

[20] M. Menon, E. Richter, A. Mavrandonakis, G. Froudakis, and A. N. Andriotis, Phys. Rev. B **69**, 115322 (2004).

[21] H. J. Xiang, Jinlong Yang, J. G. Hou, and Qingshi Zhu, Phys. Rev. B **68**, 035427 (2003).

[22] G. Y. Guo and J. C. Lin, Phys. Rev. B **71**, 165402 (2005).

[23] M. Zhao, Y. Xia, F. Li, R. Q. Zhang, and S.-T. Lee, Phys. Rev. B **71**, 085312 (2005).

[24] H. J. Xiang, Z. Y. Chen, and Jinlong Yang, J. Comput. Theor. Nanosci. **3**, 838 (2006).

[25] A. Gali, Phys. Rev. B **73**, 245415 (2006).

[26] R. J. Baierle, P. Piquini, L. P. Neves, and R. H. Miwa, Phys. Rev. B **74**, 155425 (2006).

[27] A. Gali, Phys. Rev. B **75**, 085416 (2007).

[28] C.-H. Park, C. D. Spataru, and S. G. Louie, Phys. Rev. Lett. **96**, 126105 (2006).

[29] L. Wirtz, A. Marini, and A. Rubio, Phys. Rev. Lett. **96**, 126104 (2006).

[30] D. Vogel, P. Krüger, and J. Pollmann, Phys. Rev. B **52**, R14316 (1995); **54**, 5495 (1996).

[31] D. Vogel, P. Krüger, and J. Pollmann, Phys. Rev. B **55**, 12836 (1997).

[32] B. Baumeier, P. Krüger, and J. Pollmann, Phys. Rev. B **73**, 195205 (2006).

[33] B. Baumeier, P. Krüger, and J. Pollmann, Phys. Rev. B **75**, 045323 (2007).

[34] L. Kleinman and D. M. Bylander, Phys. Rev. Lett. **48**, 1425 (1982).

[35] D. M. Ceperley and B. J. Alder, Phys. Rev. Lett. **45**, 566 (1980).

[36] J. P. Perdew and A. Zunger, Phys. Rev. B **23**, 5048 (1981).

[37] D. R. Hamann, Phys. Rev. B **40**, 2980 (1989).

[38] We use as decay constants (in atomic units) 0.18, 0.50, and 1.00 for Si, 0.25, 1.00, and 2.86 for C, 0.20, 0.42, and 1.90 for B, 0.31, 1.36, and 6.00 for N, 0.18, 0.40, and 0.90 for Be, and 0.30, 0.90, and 3.50 for O.

[39] X. Blase, A. Rubio, S. G. Louie, and M. L. Cohen, Phys. Rev. B **51**, 6868 (1995).

[40] J. Wieferink, P. Krüger, and J. Pollmann, Phys. Rev. B **74**, 205311 (2006).

[41] H. J. Monkhorst and J. D. Pack, Phys. Rev. B **13**, 5188 (1976).

[42] For the total energy, as formulated within our SIC approach (Ref. 32), the calculation of Hellmann-Feynman and Pulay forces becomes more involved than in the standard LDA approach. Since the structure parameters obtained for the bulk crystals in LDA are in good agreement with those resulting in SIC (see Table I), we refrain for the NTs from the somewhat more involved force calculations within SIC and determine their structure within standard DFT-LDA framework. For the resulting optimized structures, the total energy is then calculated within SIC and the respective total energy curve is determined.

[43] G. L. Harris, in *Properties of Silicon Carbide*, edited by G. L. Harris, EMIS Datareviews Series No. 13 (INSPEC, London, 1995).

[44] W. R. L. Lambrecht and B. Segall, in *Properties of Group III Nitrides*, edited by J. H. Edgar (EMIS Datareviews Series, London, 1994).

[45] R. W. G. Wyckoff, *Crystal Structure* (John Wiley, New York, 1963).

[46] N. Miyata, K. Moriki, O. Mishima, M. Fujisawa, and T. Hattori, Phys. Rev. B **40**, 12028 (1989).

[47] *Handbook of Laser Science and Technology*, edited by M. J. Weber (CRC, Cleveland, 1986), Vol. III.

[48] T. Miyake and S. Saito, Phys. Rev. B **68**, 155424 (2003).